†Electronic supplementary information

Substrate controls photovoltage, photocurrent and carrier separation in nanostructured Bi_2S_3 films

Sherdil Khan, [a,b] Sahar Daemi, [b] Maria Kanwal, [b] Chengcan Xiao, [b] and Frank E. Osterloh [b*]

[a] Laboratory of Nanomaterials for Renewable Energy and Artificial Photosynthesis (NanoREAP), Institute of Physics, UFRGS, Av Bento Goncalves 9500, 91509-900, Porto Alegre-RS, Brazil.

sherdil.khan@ufrgs.br

[b] Department of Chemistry, University of California, One Shields Avenue, Davis, CA 95616, USA.

*fosterloh@ucdavis.edu

† Electronic supplementary information available: *Including table for photocurrent comparison, morphological, crystallographic and surface characterizations of the substrates and the prepared films and their PEC performances.*

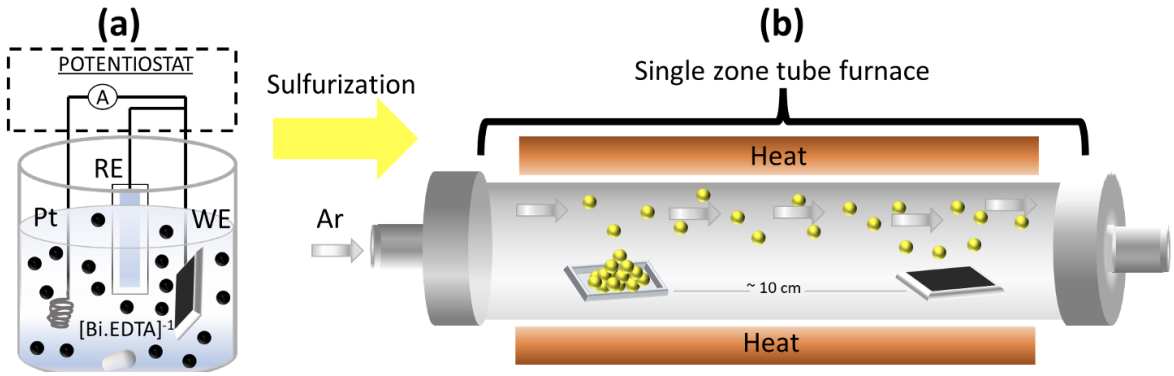

Scheme S1. Schematic representation of (a) the electrochemical deposition of Bi via reduction of Bi(III) EDTA complex ($Bi^{3+}_{(aq)} + 3\ e^- \rightarrow Bi_{(s)}$) and (b), sulfurization in a single zone tube furnace by two step heat ramping ($2\ Bi + 3\ S \rightarrow Bi_2S_3$).

Table S1. Photocurrent comparison with the previous literature based on Bi_2S_3 photoelectrodes.

	Synthesis Method	Subs.	Photoelectrode	Electrolyte	J_{max} mA cm^{-2}	Ref.
1	**Electrodeposition/ Sulfurization**	**FTO, Mo, Au, ITO**	**Bi_2S_3**	**0.5M Na_2S**	**9.3, 6.1, 3.6, 1.8**	**This work**
2	In-situ (soaking in $Bi(NO_3)_3$ solution	FTO	Bi_2S_3/WO_3	0.2M glacial acid	8	[1]
3	Modified hydrothermal	FTO	$ZnS/Bi_2S_3/ZnO$	Na_2S/Na_2SO_3	10.7	[2]

	method					
4	Hydrothermal vulcanization of sputtered Bi2O3	FTO	Bi_2S_3 nanostructures	0.2M Na_2SO_4	0.083	[3]
5	Electrochemical/ hydrothermal deposition	FTO	Bi_2S_3/CdS	0.1M Na_2SO_3	9.48	[4]
6	SILAR method	FTO	$BiVO_4$/Bi_2S_3	0.5M Na_2SO_4	2.25	[5]
7	SILAR method	Tungsten sheet	WO_3/ Bi_2S_3 QDs	0.1 M Na_2S/Na_2SO_3	16.28	[6]
8	Ion exchange method	FTO	$BiVO_4$/ Bi_2S_3/$NiCoO_2$	0.5M Na_2SO_4	3.8	[7]
9	Electrochemical/ Hydrothermal method	ITO	$BiVO_4$/Bi_2S_3	0.2M Na_2SO_4	1.1	[8]
10	SILAR method	Ti foil	Bi_2S_3/TiO_2 nanotubes	0.25M Na_2S /0.125 M Na_2SO_3	2	[9]
11	Hydrothermal reaction with precursor film	FTO	V-rich Bi_2S_3 nanowires	0.1 M Na_2S/ 0.1M Na_2SO_3	10	[10]
12	Hydrothermal/ SILAR	FTO	TiO_2/Bi_2S_3	0.1 M Na_2S and Na_2SO_3	3.98	[11]
13	SILAR/ Hydrothermal process	FTO	Bi_2O_3/ $BiVO_4$/ WO_3	0.1 M Na_2S/ 0.5M Na_2SO_3	1.52	[12]
14	Hydrothermal/ SILAR	FTO	WO_3/ Bi_2S_3	0.1 M Na_2S/ 0.1M Na_2SO_3	2.86	[13]
15	SILAR/ hydrothermal	ITO	Bi_2S_3/Ag_2S/ZnO	0.1 M Na_2S/ 0.1M Na_2SO_3	12.95	[14]
16	Two step anodization/ solvothermal method	Ti foil	TiO_2 NTs/Bi_2S_3-BiOI	0.2M Na_2SO_4	2.42	[15]
17	Hydrothermal/ in situ synthesis of Bi_2S_3 from $BiVO_4$	FTO	WO_3/ $BiVO_4$/ Bi_2S_3	0.5M Na_2SO_4 and 0.5M Na_2SO_3	2.96	[16]
18	SILAR	FTO	Bi_2S_3	Na_2S	0.8	[17]
19	Chemical bath deposition	FTO	Tip-decorated ZnO/ Bi_2S_3	0.25M Na_2S/0.35M Na_2SO_3	15.3	[18]
20	Electrodeposition/ solution deposition	ITO	$BiVO_4$/ Bi_2S_3-FeOOH	0.1M Na_2SO_4	0.8	[19]

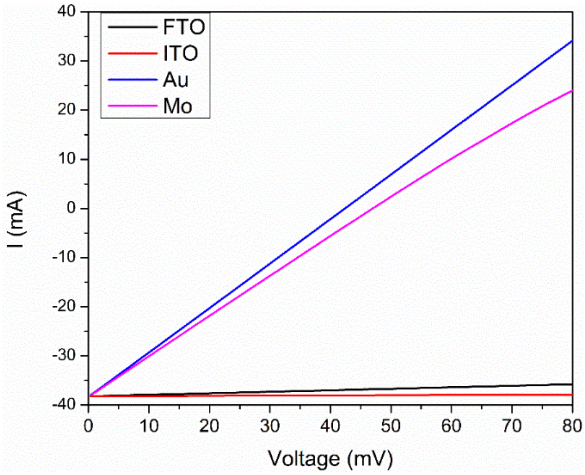

Figure S1. I-V curves of the cleaned substrates. Substrates were contacted electrically with two toothless clips placed 1.0 cm apart. Measurements were performed with Gamry (Reference 600) potentiostat at a scan rate of 0.5 mV. From the slopes of these I-V curves, the resistances were estimated as 1.1±0.1, 1.2±0.1, 33.3±0.3 and 238.1±8 Ω, for Au, Mo, FTO and ITO, respectively.

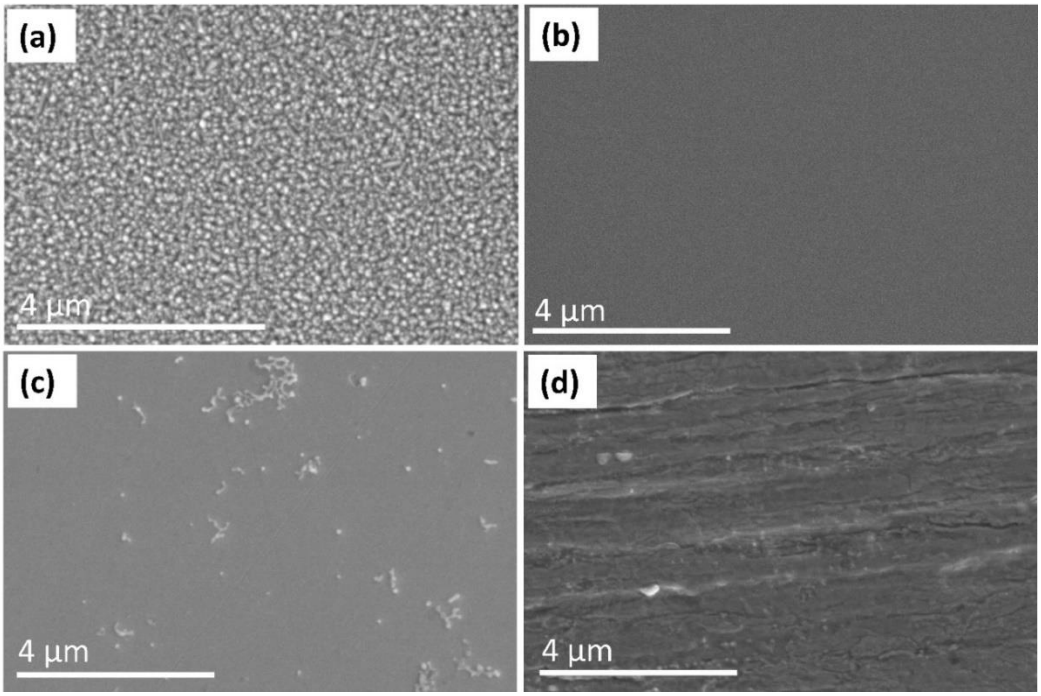

Figure S2. SEM images of (a) FTO, (b) ITO, (c) Au and (d) Mo substrates. Each substrate presents a distinct morphology with FTO being the roughest of all.

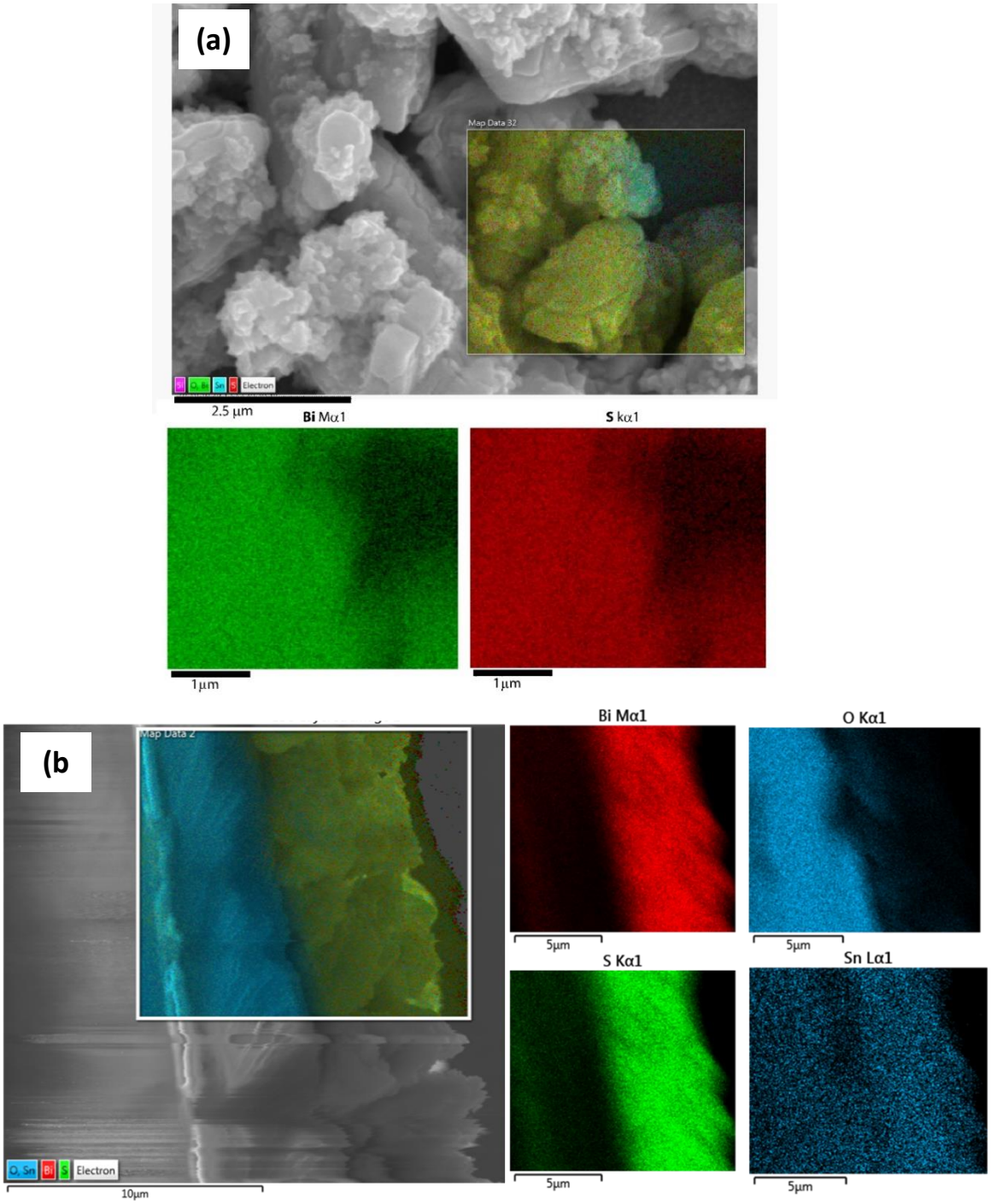

Figure S3. (a) Plain view, EDS mapping of FTO/Bi_2S_3 film, showing uniform Bi and S distribution. From the dark spot of the film, Sn signals were detected showing the pinholes are the uncovered parts of FTO, (b) EDS mapping of FTO/Bi_2S_3 film along the cross section presenting uniform Bi and S distribution.

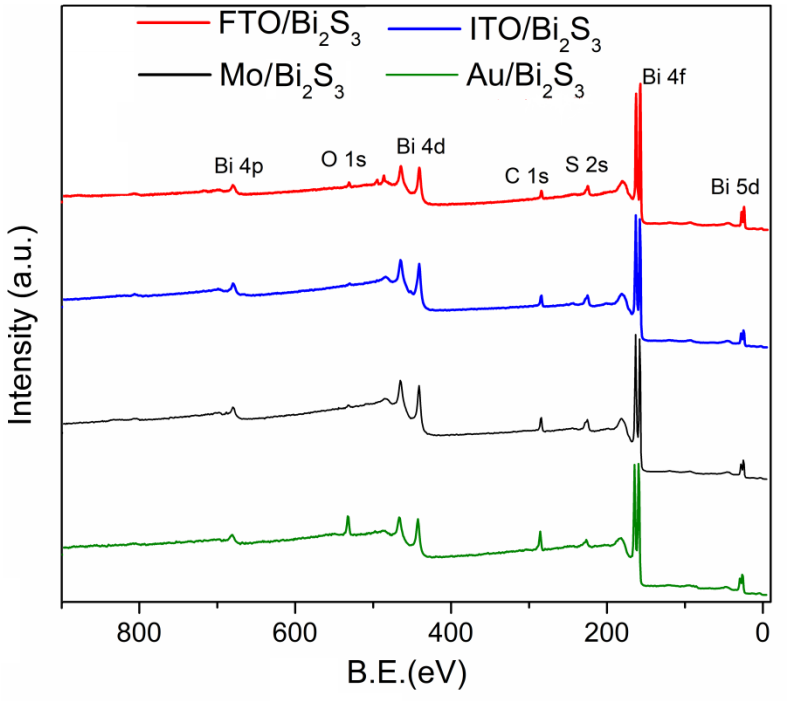

Figure S4. XPS survey spectra of the Bi_2S_3 films prepared on different substrates. Presence of Bi, S, adventitious carbon and adsorbed O species can be observed. No other species were detected in the survey spectra.

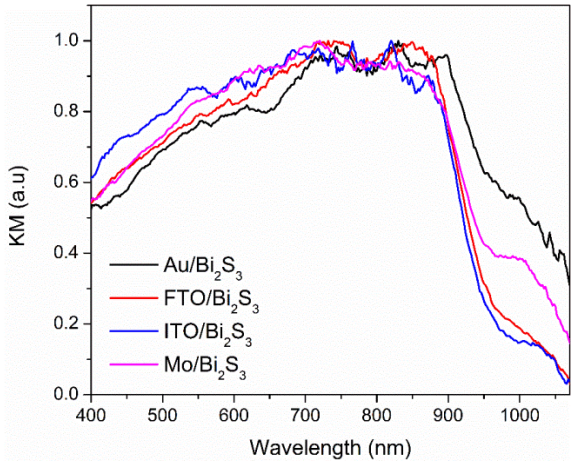

Figure S5. UV-Vis diffused reflectance spectrophotometry of Bi_2S_3 on different substrates.

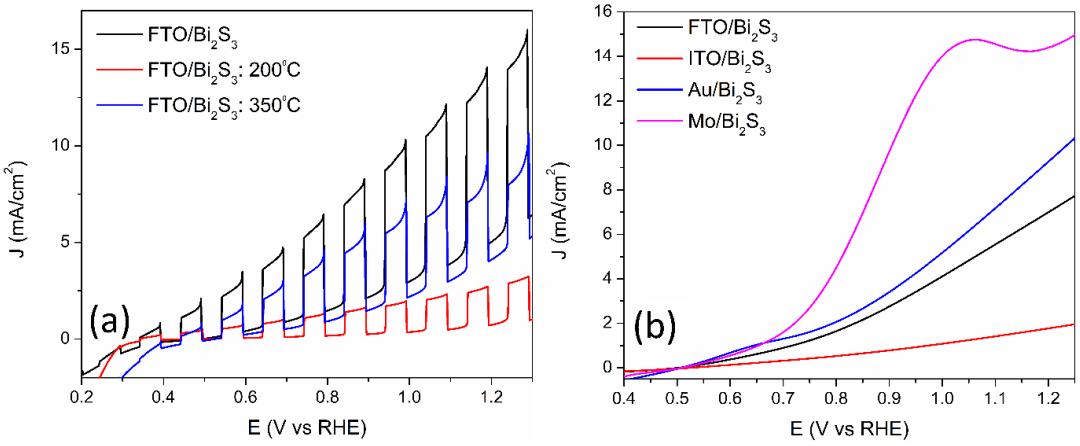

Figure S6. LSV curves (a) of FTO/Bi_2S_3 prepared by double ramping and the other prepared separately at 200°C for 3h and at 350°C for 1h and (b) in dark from Bi_2S_3 films on different substrates in 0.5 M Na_2S.

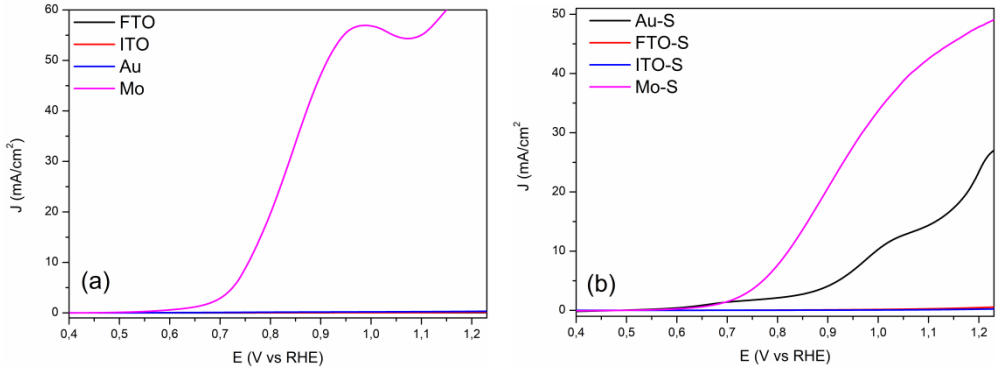

Figure S7. LSV curves of the bare substrates in 0.5 M Na_2S (a) before and (b) after sulfurization. The electrolyte was purged with N_2 flow prior to the measurements. The electrodes potentials were corrected after ohmic drop by E = Applied potential – iR and the R value for each substrate was taken from Figure S1 and S8a.

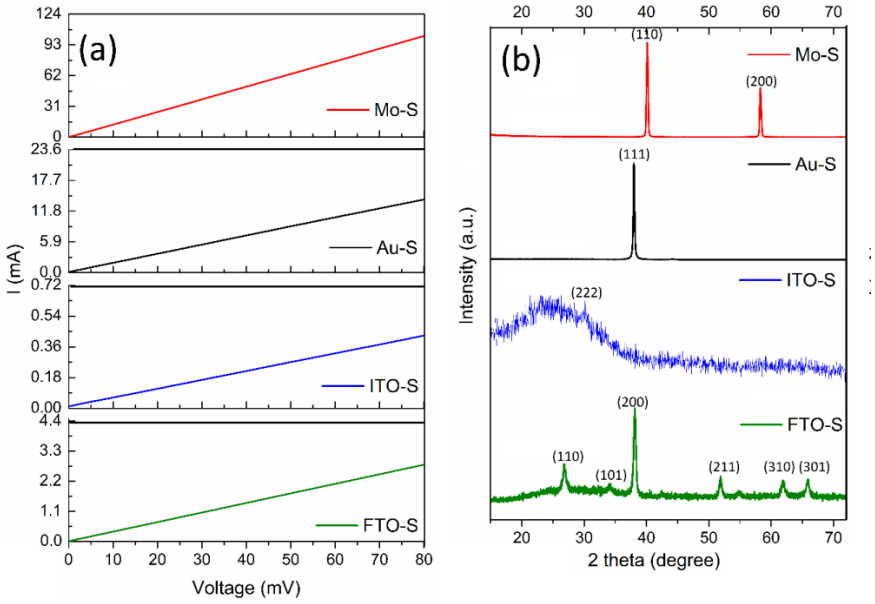

Figure S8. (a) I-V curves of the same substrates measured under similar conditions as of Figure S1. From the slopes of these I-V curves, the resistances were estimated as 5.8±0.7, 0.1±0.04, 28.6±0.4 and 200.3±10 Ω, for Au, Mo, FTO and ITO, respectively. (b) XRD patterns of the substrates sulfurized under the same heating conditions used to prepare Bi_2S_3. Miller indices are for Mo, Au, ITO, and FTO, respectively. Sulfurization does not affect the bulk substrates.

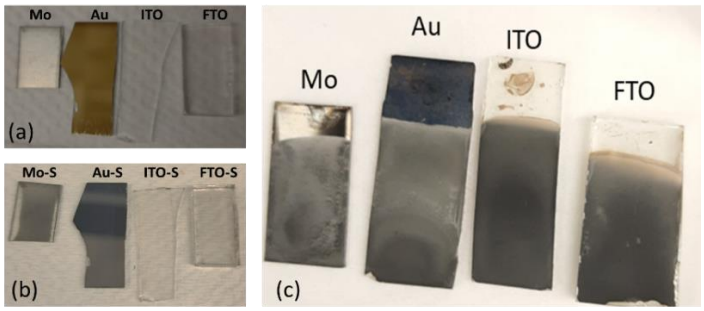

Figure S9. Photographs of the substrates before (a) and after sulfurization (b). While FTO and ITO appear unchanged, the Mo and Au substrates change color to a grey-brown from the presence of a sulfide overlayer. (c) Photographs of Bi_2S_3 films on different substrates.

To verify if there exists any substrate related sulfurized species, XRD was also performed from the substrates sulfurized at the same heating conditions used for the preparation of Bi_2S_3 films (Figure S8b). The XRD patterns for Mo, Au and FTO substrates match well with JCPDS# 421120, 4784 and 77448, respectively which correspond to their standard diffraction peaks. For ITO, only a weak peak at $2\theta = 30.7°$ was observed which is its characteristic peak in JCPDS# 6416, the reason to lower intensity may be the film thickness. No additional peaks other than the substrate peaks were observed in the diffractograms after sulfurization. Interestingly, the sulfurized substrates presented changes in their resistances (Figure S8a) compared to their un-sulfurized counterparts (Figure S1) which confirms the substrate surface reactivity with S. Photos are also displayed to compare the colour differences before and after sulfurization (Figure S9). Some colour changes were observed; particularly, for Mo and Au. However, FTO and ITO had remained transparent but slightly less as compared to un-sulfurized FTO and ITO. These results collectively suggest that the surface of all substrates might have been reacted with sulfur during sulfurization but in the bulk, they possess similar crystal structure as that of un-sulfurized substrates.

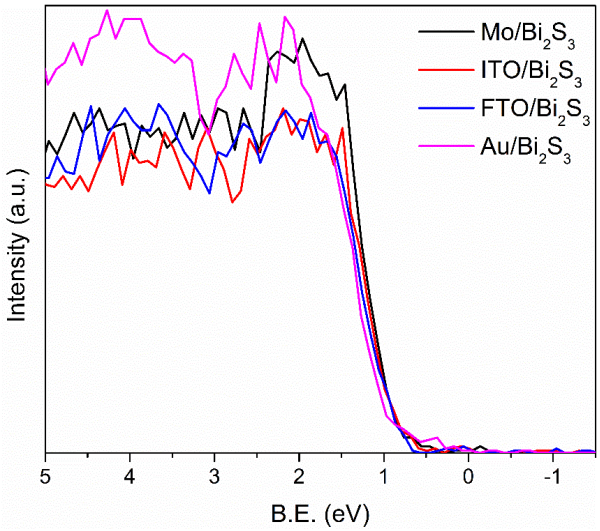

Figure S10. XPS VB spectra of Bi_2S_3 films on different substrates showing the VB edge was not influenced by the substrate.

Table S2. Parameters obtained from the circuit fitting of the electrochemical impedance spectroscopy for Bi_2S_3 on different substrates.

Sample	**R_s (Ω)**	**R_p (Ω)**	**CPE**		**C (F)**	**R_c (Ω)**
			n	**Y_0 ($10^{-3} \times \Omega^{-1}$)**		
FTO/Bi_2S_3	21.7	191.1	0.82	3.2	-	-
ITO/Bi_2S_3	194.6	316.2	0.64	2.2	-	-
Mo/Bi_2S_3	5.8	174.0	0.83	4.2	-	-
Au/Bi_2S_3	24.6	38.0	0.88	6.9	0.38×10^{-3}	56.8

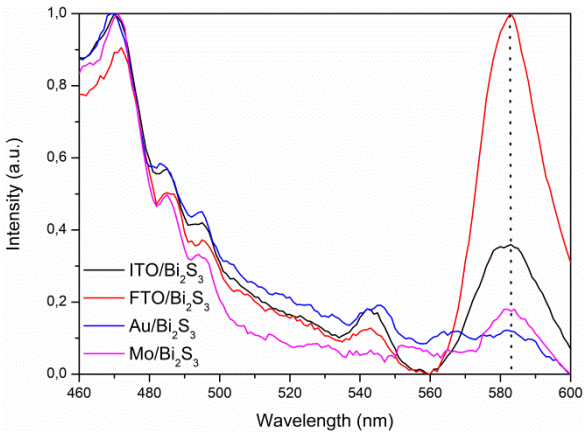

Figure S11. PL spectra of Bi_2S_3 as a function of different substrates. The dotted line represents the main emission peak

References

(1) Liu, C.; Yang, Y.; Li, W.; Li, J.; Li, Y.; Chen, Q. In Situ Synthesis of Bi2S3 Sensitized WO3 Nanoplate Arrays with Less Interfacial Defects and Enhanced Photoelectrochemical Performance. *Sci. Rep.* **2016**, *6* (1), 23451. https://doi.org/10.1038/srep23451.

(2) Lu, Y.; Popescu, R.; Gerthsen, D.; Feng, Y.; Su, W.-R.; Hsu, Y.-K.; Chen, Y.-C. Highly Efficient Recovery of H2 from Industrial Waste by Sunlight-Driven Photoelectrocatalysis over a ZnS/Bi2S3/ZnO Photoelectrode. *ACS Appl. Mater. Interfaces* **2022**, *14* (6), 7756–7767. https://doi.org/10.1021/acsami.1c18142.

(3) Liang, Y.-C.; Li, T.-H. Controllable Morphology of Bi2S3 Nanostructures Formed via Hydrothermal Vulcanization of Bi2O3 Thin-Film Layer and Their Photoelectrocatalytic Performances. **2022**, *11* (1), 284–297. https://doi.org/10.1515/ntrev-2022-0016.

(4) Yang, M.; Shi, Y.; Li, Y.; Li, H.; Luo, N.; Li, J.; Fan, J.; Zhou, A. Construction of 2D Bi2S3/CdS Nanosheet Arrays for Enhanced Photoelectrochemical Hydrogen Evolution. *J. Electron. Mater.* **2019**, *48* (10), 6397–6405. https://doi.org/10.1007/s11664-019-07447-5.

(5) Majumder, S.; Quang, N. D.; Kim, C.; Kim, D. Anion Exchange and Successive Ionic Layer Adsorption and Reaction-Assisted Coating of BiVO4 with Bi2S3 to Produce Nanostructured Photoanode for Enhanced Photoelectrochemical Water Splitting. *J. Colloid Interface Sci.* **2021**, *585*, 72–84. https://doi.org/10.1016/j.jcis.2020.11.081.

(6) Abouelela, M. M.; Kawamura, G.; Tan, W. K.; Matsuda, A. Anodic Nanoporous WO3 Modified with Bi2S3 Quantum Dots as a Photoanode for Photoelectrochemical Water Splitting. *J. Colloid Interface Sci.* **2023**, *629*, 958–970. https://doi.org/10.1016/j.jcis.2022.09.041.

(7) Majumder, S.; Gu, M.; Hyeon Kim, K. Facile Fabrication of BiVO4/Bi2S3/NiCoO2 for Significant Photoelectrochemical Water Splitting. *Appl. Surf. Sci.* **2022**, *574*, 151562. https://doi.org/10.1016/j.apsusc.2021.151562.

(8) Li, F.; Leung, D. Y. C. Highly Enhanced Performance of Heterojunction Bi2S3/BiVO4 Photoanode for Photoelectrocatalytic Hydrogen Production under Solar Light Irradiation. *Chem. Eng. Sci.* **2020**, *211*, 115266. https://doi.org/10.1016/j.ces.2019.115266.

(9) Zeng, Q.; Bai, J.; Li, J.; Li, Y.; Li, X.; Zhou, B. Combined Nanostructured Bi2S3/TNA Photoanode and Pt/SiPVC Photocathode for Efficient Self-Biasing Photoelectrochemical Hydrogen and Electricity Generation. *Nano Energy* **2014**, *9*, 152–160. https://doi.org/10.1016/j.nanoen.2014.06.023.

(10) Geng, Y.-Y.; Tao, C.-L.; Duan, S.-F.; San Martin, J.; Lin, Y.; Zhu, X.; Zhang, Q.-Q.; Kang, X.-W.; He, S.-S.; Zhao, Y.-X.; Li, X.; Niu, L.; Qin, D.-D.; Yan, Y.; Han, D.-X. V-Rich Bi2S3 Nanowire with Efficient Charge Separation and Transport for High-Performance and Robust Photoelectrochemical Application under Visible Light. *Front. Catal. Energy Fuels Catal. Synth. Prod. Yield* **2020**, *350*, 47–55. https://doi.org/10.1016/j.cattod.2019.08.008.

(11) Ahmad, A.; Tezcan, F.; Yerlikaya, G.; Zia-ur-Rehman; Paksoy, H.; Kardaş, G. Three Dimensional Rosette-Rod TiO2/Bi2S3 Heterojunction for Enhanced Photoelectrochemical Water Splitting. *J. Alloys Compd.* **2021**, *868*, 159133. https://doi.org/10.1016/j.jallcom.2021.159133.

(12) Sadhasivam, S.; Anbarasan, N.; Gunasekaran, A.; Mukilan, M.; Jeganathan, K. Bi2S3 Entrenched BiVO4/WO3 Multidimensional Triadic Photoanode for Enhanced Photoelectrochemical Hydrogen Evolution Applications. *Int. J. Hydrog. Energy* **2022**, *47* (32), 14528–14541. https://doi.org/10.1016/j.ijhydene.2022.02.199.

(13) Zhao, F.; Sheng, H.; Sun, Q.; Wang, J.; Liu, Q.; Hu, Z.; He, B.; Wang, Y.; Li, Z.; Liu, X. Harvesting the Infrared Part of Solar Light to Promote Charge Transfer in Bi2S3/WO3 Photoanode for Enhanced Photoelectrochemical Water Splitting. *J. Colloid Interface Sci.* **2022**, *621*, 267–274. https://doi.org/10.1016/j.jcis.2022.04.052.

(14) Al-Zahrani, A. A.; Zainal, Z.; Talib, Z. A.; Lim, H. N.; Holi, A. M.; Bahrudin, N. N. Enhanced Photoelectrochemical Performance of Bi2S3/Ag2S/ZnO Novel Ternary Heterostructure Nanorods. *Arab. J. Chem.* **2020**, *13* (12), 9166–9178. https://doi.org/10.1016/j.arabjc.2020.10.040.

(15) Wang, Q.; Liu, Z.; Feng, H.; Jin, R.; Zhang, S.; Gao, S. Engineering Bi2S3/BiOI p-n Heterojunction to Sensitize TiO2 Nanotube Arrays Photoelectrodes for Highly Efficient Solar

Cells and Photocatalysts. *Ceram. Int.* **2019**, *45* (3), 3995–4002. https://doi.org/10.1016/j.ceramint.2018.11.075.
(16) Guo, H.; Zhang, Y.; Wang, S.; Li, L.; Wang, W.; Sun, Q. In-Situ Generation of Bi2S3 to Construct WO3/BiVO4/Bi2S3 Heterojunction for Photocathodic Protection of 304SS. *J. Electroanal. Chem.* **2022**, *907*, 116033. https://doi.org/10.1016/j.jelechem.2022.116033.
(17) Wang, Y.; Chen, J.; Jiang, L.; Sun, K.; Liu, F.; Lai, Y. Photoelectrochemical Properties of Bi2S3 Thin Films Deposited by Successive Ionic Layer Adsorption and Reaction (SILAR) Method. *J. Alloys Compd.* **2016**, *686*, 684–692. https://doi.org/10.1016/j.jallcom.2016.06.065.
(18) Sun, X.; Wu, H.; Tang, Y.; Zheng, Z.; Li, Y.; Li, L.; Zhang, Q. Enhanced Photoelectrocatalytic Degradation of Tetrabromobisphenol a from Tip-Decorated ZnO Nanorod Electrode with Bi2S3 Nanoparticles. *Mater. Sci. Semicond. Process.* **2021**, *128*, 105724. https://doi.org/10.1016/j.mssp.2021.105724.
(19) Wang, M.; Wang, Q.; Guo, P.; Jiao, Z. In Situ Fabrication of Nanoporous BiVO4/Bi2S3 Nanosheets for Enhanced Photoelectrochemical Water Splitting. *J. Colloid Interface Sci.* **2019**, *534*, 338–342. https://doi.org/10.1016/j.jcis.2018.09.056.